Paper ID: 359

A Numerical Study of Multiphase Flow Boiling Heat Transfer of Nanofluids in Various Porous Media of Vertical Tubes

Tahsin Enam[1], Maria Khatun[1], Saad Been Mosharof[1]
[1]Department of Mechanical Engineering, Shahjalal University of Science and Technology (SUST), Sylhet.
E-mail: tahsinenam2121@gmail.com

Abstract

This computational study examines how varying porosity and pore density in vertical tubes, which contain aluminium and copper metal foams, affect the flow boiling behavior of various nanofluids. To investigate water-based nanofluids with alumina and copper oxide nanoparticles alongside plain water as a baseline, mass flow inlet and pressure outlet boundary conditions are employed in the simulation along with heat flux to the pipe wall. This work utilizes CFD analysis using RANS equations and the RPI boiling model with Eulerian-Eulerian approach for each phase, along with the standard k-ω turbulence model to simulate subcooled nanofluid flow boiling. The study demonstrates that porous copper tubes exhibit superior thermal performance to aluminium tubes, and further identifies a significant enhancement in heat transfer when nanoparticles are added to the base water. In addition, substantial increment is also noted in heat transfer coefficient due to moderate porosity and greater pore density. Ultimately, the simulations identify an optimal foam configuration that achieves a balance between improved heat transfer and manageable pressure drop.

Keywords: CFD, Multiphase, Porous, Nanofluid.

1. Introduction

The use of nanofluid and incorporation of metallic porous media as a passive method for improving thermal conductivity in multiphase systems has gained much attention among researchers. [1] Boiling heat transfer is utilized in numerous manufacturing procedures and applications, including refrigeration, power production, solar thermal systems, heat exchangers, nuclear reactor cooling, chemical and metal processing etc. [2] Enhancements in flow boiling heat thermal technologies can boost power efficiency and provide a pathway to lowering worldwide energy usage.

Abedini et al. [3] found through experimental study that with increasing TiO_2 nanoparticles in water-based nanofluid, the subcooled flow boiling decreases. With increment in nanoparticle concentration, the heated surface becomes coated with a layer of nanoparticle. As more TiO_2 particles deposit, it reduces the contact angle and bubble emission frequency, which ultimately lessens the heat transfer coefficient. Flow boiling of γ-Al_2O_3/H_2O nanofluid of 0.1 and 0.5% volume fraction was experimentally tested in a vertical tube by Wang et al. [4]. They recorded an average heat transfer enhancement of around 35% with a maximum enhancement of 86%, relative to that of pure water. The formation of sedimentary layer led to this conclusion since the dimensions of nanoparticles is much less than the nucleation sites and surface roughness which are in micrometer range. Hence, the deposition of nanoparticle reduces the number of nucleating sites and roughness, which negatively impacts the heat transfer process. Experimental work was done by Jaganathan et al. [5] to study water-based TiO_2 nanoparticle of varying volume concentrations (0.025, 0.05, 0.1 and 0.2%) and temperatures at inlet (40, 50, and 60° C) flowing within fin channels. When compared to pure water, the highest increase in heat transfer coefficient is recorded at 48.2 and they also found that maximum pressure drop of roughly 2.7% occurs at 0.2% concentration when temperature at inlet is 40° C. The reduction in coefficient of heat transfer past concentration of 0.05% was attributed to the dampening of turbulence intensity. As nanoparticle of higher concentration is added, the viscosity of nanofluid increases and this creates a surge in shear stress at wall. Ultimately, the boundary layer thickness of velocity reduces and drop of pressure heightens.

Numerical study of flow boiling of Al_2O_3/water and ZrO_2/water nanofluids at varying concentrations (0.1, 0.01 and 0.001%) conducted by Hasheminia et al. [6] reported inverse relation between coefficient of boiling heat transfer and concentration of nanoparticles. At 0.01% volume fraction, ZrO_2/water and Al_2O_3/water shows 31% (maximum) and 11% (minimum) heat transfer enhancement respectively when compared to base fluid. They

reasoned that for Al_2O_3/water, the contact angle increases with rise in concentration which ultimately increases heat transfer whilst the opposite occurs in case of ZrO_2/water. Das et al. [7] carried out experimental studies in a horizontal tube on the performance of the boiling process of water based nanofluids. They noticed that prominent change occurs in boiling when roughened heater with fewer particle concentration is used. With higher surface roughness (1.15 micrometer), there are greater voids on the surface and hence the leveling of the surface by sedentary particles is more irregular. Thus, particle concentrations of <1% deposit enough particles on rough surfaces to significantly impact boiling characteristics. Experimental investigation of flow of water-based Fe_3O_4 nanofluid in a metal foam pipe conducted by Amani et al. [8], resulted in no more than 11.7% heat transfer enhancement due to 1% volume fraction of nanoparticles. They stated that key factors behind this increment is the surge of nanoparticle Brownian motion which results in more non-uniform particle distribution and migration within the base fluid. An investigation was conducted by Dukhan et al. [9] numerically to enhance heat transfer in forced convection within a tube partially filled with porous media, positioned both at the center and near the wall of the pipe. They recorded that better and lower heat transfer occurs when foam is positioned at the core and near the wall of the pipe respectively. Ghafarian et al. [10] used metal foam to numerically carry out study of forced convection within a channel. In order to do so, they placed the foam at the center of the channel and cooling was done by two coolers on two sides while being subjected to constant heat flux. The results recorded an increase in heat transfer at 0.9 porosity and reduced pressure drop at 10 PPI of metal foam. As metal foams offer a large ratio of surface area to volume, this ultimately aids in reducing thermal resistance and enhancing the overall transfer of heat. Azizifar et al. [11] examined water-based nanofluid undergoing flow boiling in a horizontal metallic foam pipe, finding that it boosts heat transfer by 3.5–5.8 times relative to a plain pipe. They stated that contact thermal resistance between tube wall and metal foam structure as well as foam constraints such as holes and ligaments negatively impact the heat transfer process as they limit bubble movement.

As seen above, there remains a significant gap in research regarding the influence of porous media in flow boiling heat transfer process. This present work aims to address this through the investigation of flow boiling of Al_2O_3/H_2O and CuO/H_2O nanofluids in aluminium and copper vertical porous tubes. Hence, three distinct pore densities and porosities are employed and the resultant coefficient of heat transfer and pressure loss are discussed. It also provides a better understanding of achieving an optimal foam configuration using the aforementioned parameters.

2. Methodology

Geometry and boundary conditions

A tube of length 2000 mm and diameter 15.7 mm of aluminium and copper foam is used with three different porosities (0.8, 0.85 and 0.9) and pore density (5, 10 and 20 PPI). For the two-dimensional axisymmetric geometry, mass flow inlet (0.167 kg/s) and pressure outlet boundary conditions are employed along with heat flux of 570000 W/m^2 to the pipe wall. The inlet temperature, saturation temperature and operating pressure are 473K, 530.44 K and 45 bar respectively. Fig. 1 shows the tube schematic.

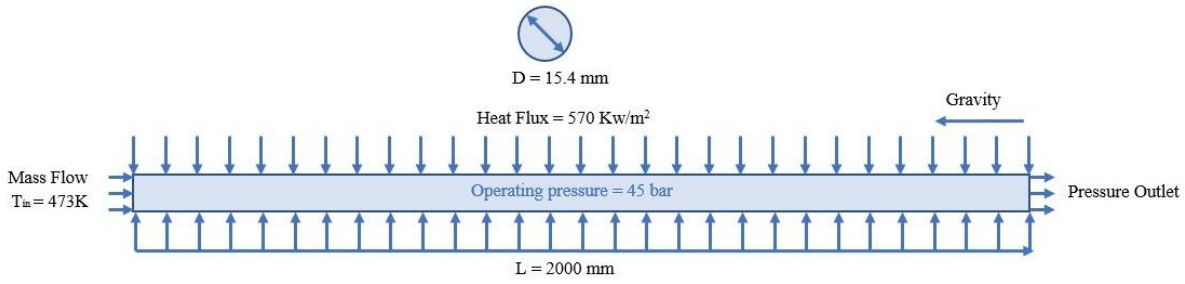


Fig. 1. Geometry and boundary conditions

CFD model

Governing equations for mass, momentum and energy transport equations can be written as: [12]
Mass equation of water-based nanofluid

$$\frac{\partial \rho_{l,eff}\alpha_l}{\partial t} + \nabla.(\rho_l \alpha_l \vec{u_l}) = \Gamma_{lg} \quad (1)$$

Mass equation of vapor

$$\frac{\partial \rho_g \alpha_g}{\partial t} + \nabla.\left(\rho_g \alpha_g \overrightarrow{u_g}\right) = \Gamma_{gl} \tag{2}$$

Momentum equation of water-based nanofluid

$$\frac{1}{\gamma}\left(\frac{\partial \rho_{l,eff} \alpha_l \overrightarrow{u_l}}{\partial t}\right) + \left(\frac{1}{\gamma}\right)\nabla.\left(\rho_{l,eff} \alpha_l \overrightarrow{u_l}\overrightarrow{u_l}\right) = -\alpha_l \nabla p + \gamma \rho_{l,eff}\, \alpha_l \vec{g} + \frac{1}{\gamma}\nabla\left[\alpha_l \mu_l^e (\nabla \overrightarrow{u_l} + (\nabla \overrightarrow{u_l})^T)\right] + \gamma\left(\Gamma_{lg}\, \overrightarrow{u_g} - \Gamma_{gl} \overrightarrow{u_l}\right) + F_{lg} + \left(\frac{\mu_l}{K_p} + \frac{\rho_l C |u_l|}{\sqrt{K_p}}\right)\overrightarrow{u_l} \tag{3}$$

Momentum equation of vapor

$$\frac{1}{\gamma}\left(\frac{\partial \rho_g \alpha_g \overrightarrow{u_g}}{\partial t}\right) + \left(\frac{1}{\gamma}\right)\nabla.\left(\rho_g \alpha_g \overrightarrow{u_g}\overrightarrow{u_g}\right) = -\alpha_g \nabla p + \gamma \rho_g\, \alpha_g \vec{g} + \frac{1}{\gamma}\nabla\left[\alpha_g \mu_g \left(\nabla \overrightarrow{u_g}\right)\right] + \gamma\left(\Gamma_{gl}\, \overrightarrow{u_l} - \Gamma_{lg} \overrightarrow{u_g}\right) + F_{gl} + \left(\frac{\mu_g}{K_p} + \frac{\rho_g C |u_g|}{\sqrt{K_p}}\right)\overrightarrow{u_g} \tag{4}$$

Energy equation of water-based nanofluid

$$\frac{\partial \rho_{l,eff} \alpha_l H_l}{\partial t} + \nabla.\left(\rho_{l,eff} \alpha_l \vec{u}_l H_l\right) = \nabla\left[\alpha_l k_l^e (\nabla T_l)\right] + (\Gamma_{gl} H_l - \Gamma_{lg} H_g) \tag{5}$$

Energy equation of vapor

$$\frac{\partial \rho_g \alpha_g H_g}{\partial t} + \nabla.\left(\rho_g \alpha_g \overrightarrow{u_g} H_g\right) = \nabla\left[\alpha_g k_g \left(\nabla T_g\right)\right] + (\Gamma_{lg} H_g - \Gamma_{gl} H_l) \tag{6}$$

The governing equation for the transport of k and ω are defined by these equations: [13]

$$\frac{\partial}{\partial t}(\rho k) + \frac{\partial}{\partial x_j}\left(\rho u_j k\right) = \rho \tau_{ij} \frac{\partial u_i}{\partial x_j} - \beta \rho k \omega + \frac{\partial}{\partial x_j}\left[\left(\mu + \sigma \frac{\rho k}{\omega}\right)\left(\frac{\partial k}{\partial x_j}\right)\right] \tag{7}$$

$$\frac{\partial}{\partial t}(\rho \omega) + \frac{\partial}{\partial x_j}\left(\rho u_j \omega\right) = \alpha \frac{\omega}{k} \rho \tau_{ij} \frac{\partial u_i}{\partial x_j} - \beta \rho \omega^2 + \frac{\sigma_d \rho}{\omega} \frac{\partial k}{\partial x_j} \frac{\partial \omega}{\partial x_j} + \frac{\partial}{\partial x_j}\left[\left(\mu + \sigma \frac{\rho k}{\omega}\right)\left(\frac{\partial \omega}{\partial x_j}\right)\right] \tag{8}$$

The following correlations are used for calculating the viscous resistance (α), inertial resistance (C_2) and pore diameter (d_p) where ω is pore per inch (PPI) and ϵ is porosity: [14]

$$\alpha = \frac{D_p^2}{150} \frac{\epsilon^3}{(1-\epsilon)^2}, C_2 = \frac{3.5}{D_p} \frac{1-\epsilon}{\epsilon^3}, d_p = \frac{0.0254}{\omega(PPI)} \tag{9}$$

The calculation of overall heat transfer coefficient is done using the constant heat flux at wall of the tube (q) and the difference in wall temperature and bulk liquid temperature (ΔT): [15]

$$h = \frac{q}{\Delta T} \tag{10}$$

For solving technique, RANS equations and the RPI boiling model is utilized with Eulerian-Eulerian approach for two phases to simulate subcooled nanofluid flow boiling. It is also assumed that liquid phase properties change with temperature while vapor phase properties are taken as constant at saturation temperature.

Grid independency test

The following computational grids were analyzed to achieve mesh-independency. 25200 elements are used as the optimal mesh size for all numerical simulation since the change in subsequent values is only 1.82%. Using 25200 elements resulted in improved efficiency and reduced computational time.

Table 1. Mesh element number and corresponding pressure drop

Element No.	10000	25200	30000	54000	81200	93000
Pressure Drop (kPa)	119	110	109	109	108	109

3. Validation

The numerical study carried out by Rabiee et al. [16] of flow boiling of water within a tube of length 2 m and

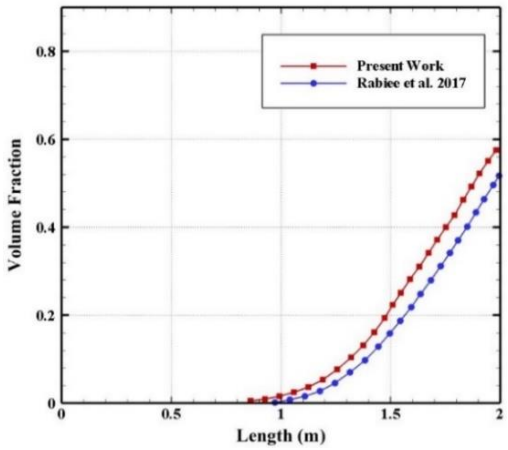


Fig. 2. Variation of volume fraction with respect to porosity

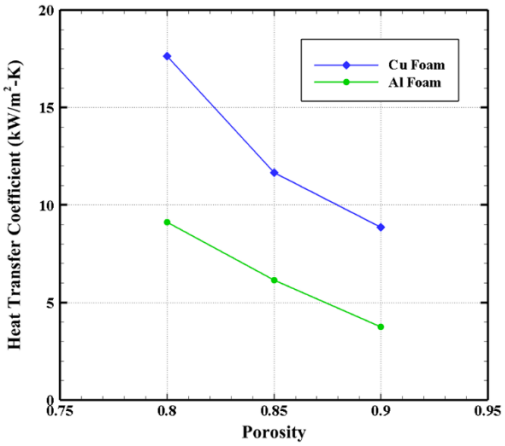


Fig. 3. Variation of heat transfer coefficient with respect to porosity

diameter 15.7 mm is used as the primary validation case. Fig. 2 demonstrates the variation of vapor volume fraction with respect to length of the tube. The results of the current study are shown relative to the numerical outcomes from the validation case. There exists acceptable agreement between the two data. The maximum error is about 15% and the most deviation can be seen after a length of 1.5 m.

4. Results

In order to examine the flow boiling of CuO/H_2O and Al_2O_3/H_2O nanofluid, the aforementioned validation case with constant heat flux has been taken. Same pipe dimension, mass flow rate, operating pressure, and heat flux are employed for further investigation and ease of calculation.

Flow boiling within both aluminium and copper tube of varying porosity and pore density for 0.01% nanoparticle volume fraction and 0.001 granular temperature are simulated. The diameter of nanoparticle is 10 nm.

Effect of foam tube

Two distinct metallic foam tubes are utilized to compare the variance in heat transfer coefficients due to tube material. Copper and aluminium have different thermophysical properties, which affect the heat transmission performance of various nanofluids. It emphasizes and explains the distinct influence of each substance.

Fig. 3 shows that heat transfer coefficient is much higher for copper tube compared to aluminium tube. For metal foam with lower thermal conductivity, heat transfer into the foam does not occur efficiently which causes energy to accumulate in the tube and increase the surface temperature. Ultimately, both convection and evaporation heat transfer from solid to liquid then liquid onto vapor decreases. The contrary occurs for copper foam which results in better heat distribution, improved nucleate boiling and reduced thermal boundary layer which consequently enhances the overall heat transfer process. Hence at 0.8 porosity and 20 PPI, the heat transfer coefficient of Cu foam is 93% greater than that of Al foam. This difference is lesser at a higher porosity as the coefficient of heat transfer of Cu foam is 82% greater than Al foam at 0.9 porosity and 20 PPI.

Effect of porosity and pore density

Fig. 4 (a) and (b) highlight the vapor volume fraction contour of Al_2O_3/H_2O nanofluid flow boiling in copper foam for 5 PPI at 0.8 and 0.9 porosity respectively. In the former case, the vapor formation is witnessed at a length of 1500 mm and in the latter case, it occurs at a nearer distance of around 1200 mm. This concludes that for higher porosity, the bubble formation occurs earlier. At pipe inlet, the fluid flow is single-phase and as more heat from pipe wall is transferred to the fluid, saturation temperature of 530.44 K is achieved and boiling process begins.

Fig. 5 shows the heat transfer coefficient of CuO/H_2O nanofluid in copper foam tube. With greater porosity under alike pore density, the solid ligaments that separate the pores become thinner thus causing amplified thermal resistance of conduction heat transfer. Moreover, with lower pore density, the available pathways for nanofluid to interact with the foam structure is diminished. Both of these combinedly, reduce the heat transfer coefficient. Thus at 0.8 porosity, 11.42% higher heat transfer coefficient is found at 20 PPI compared to 5 PPI.

However, in Fig. 6 the pressure drop for CuO/H_2O nanofluid in copper foam tube is shown. It is noted that for higher porosity and lower pore density, there occurs lesser drop in pressure. Because of the combined effect of reduction in porous structure as well as number of pores, there exists less resistance in flow direction. The increased pore number causes frictional resistance and flow separation that contributes to additional pressure loss. Moreover, more pores also introduce greater surface roughness that is a huge factor in overall pressure drop. At 0.8 porosity, the pressure is 70.83% greater at 20 PPI compared to its corresponding value at 5 PPI.

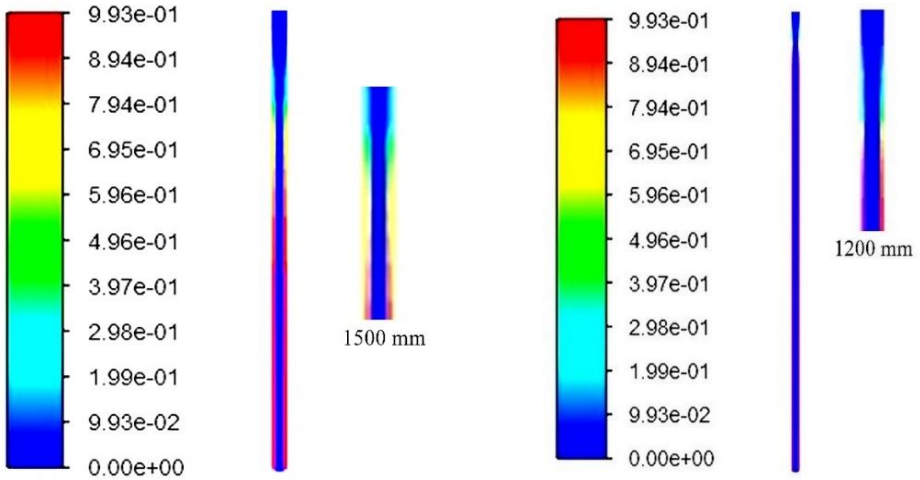


Fig. 4. Vapor volume fraction contour at (a) 0.8 porosity and 5 PPI and (b) 0.9 porosity and 5 PPI

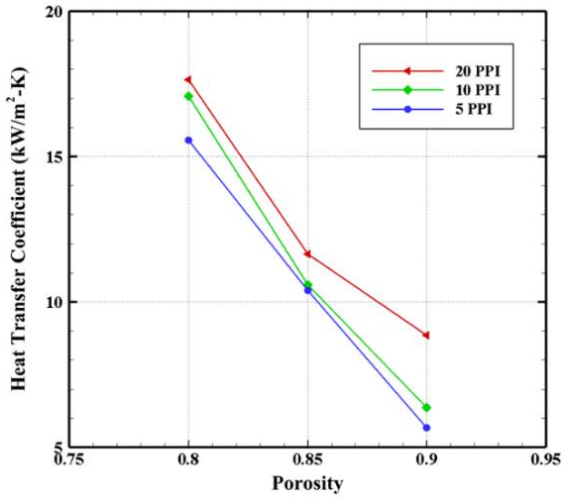


Fig. 5. With respect to porosity variation of heat transfer coefficient for CuO/H₂O nanofluid

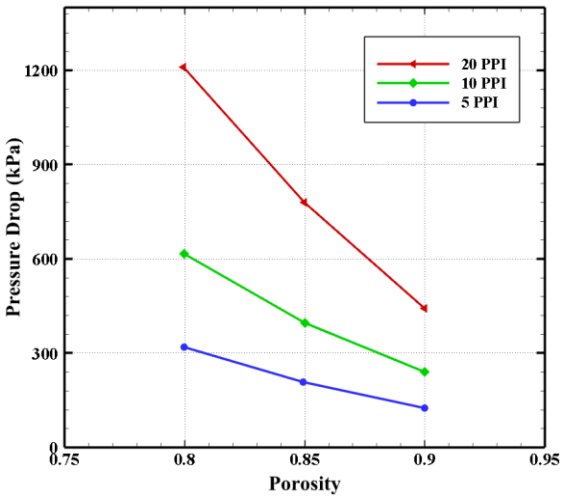


Fig. 6. Variation of pressure drop with respect to porosity for CuO/H₂O nanofluid

Performance evaluation

In order to find the optimum foam configuration, the simultaneous impact of the drop in pressure and heat transfer increment are evaluated using the following equation where h_1, Δp_1 and h_2, Δp_2 are heat transfer coefficient and pressure drop of CuO/H₂O and Al₂O₃/H₂O nanofluids respectively.

$$\eta = \frac{\frac{h_1}{h_2}}{\frac{\Delta p_1}{\Delta p_2}} \tag{11}$$

Fig. 7 shows the variation of performance index with respect to porosity for flow boiling of CuO/H₂O and Al₂O₃/H₂O nanofluid in copper foam. It can be seen that in general, CuO/H₂O nanofluid performs better. CuO/H₂O nanofluid have lower contact angle compared to Al₂O₃/H₂O nanofluid which causes high wettability. As liquid spreads and comes more in contact with heated surface, efficient heat transfer occurs due to formation of more nucleation sites. However, at higher pore density, the value of performance index is less than 1 implying that Al₂O₃/H₂O nanofluid shows better trade-off between enhanced heat transfer coefficient and pressure drop. At higher pore density, the fluid navigates through smaller pores and since CuO nanofluid have higher viscosity it amplifies the pressure drop and hence performance index falls below 1. The maximum performance index of 1.08 is found for 0.9 porosity at 5 PPI and the minimum performance is 0.93 for 0.85 porosity at 20 PPI. This reiterates the importance of achieving balance between lower pore density and higher porosity when it comes to optimal foam configurations.

Table 2. Heat transfer coefficient and pressure drop of CuO/H_2O and Al_2O_3/H_2O at varying porosity and PPI

PPI	Porosity	Heat Transfer Coefficient (Al_2O_3/H_2O)	Pressure Drop (Al_2O_3/H_2O)	Heat Transfer Coefficient (CuO/H_2O)	Pressure Drop (CuO/H_2O)
20	0.8	17.4	1180	17.63	1210
	0.85	12.04	753	11.65	777
	0.9	6.84	441	6.86	445
10	0.8	19.64	679	17.08	616
	0.85	10.25	387	10.57	396
	0.9	5.87	232	6.36	238
5	0.8	15.16	306	15.56	317
	0.85	9.88	202	10.38	205
	0.9	5.32	127	5.68	126

5. Conclusion

This study carries out CFD simulations of a vertical metal foam pipe (copper and aluminium) through which different nanofluids (CuO, Al_2O_3) are flown. As phase change of water to vapor takes place, the coefficient of heat transfer and pressure drop are studied taking into account the combined effect of foam and nanoparticle. Furthermore, the thermal performance on the effect of different foam structure according to pore density of 5, 10, 20 PPI and 0.8, 0.85, 0.9 porosity is also analyzed in this work. Additionally, the comparative thermal performance between different nanofluids as well as copper and aluminium foam is also demonstrated. The numerical results show that for lower porosity, both the pressure drop and coefficient of heat transfer increases significantly. Similarly, for increasing pore density there occurs a prominent rise in pressure drop and heat transfer coefficient. However, compared to the pressure loss, the surge in coefficient of heat transfer is insignificant. Hence comparing the results using performance index, CuO/ H_2O nanofluid in copper foam with 5 PPI and 0.9 porosity shows better thermal performance.

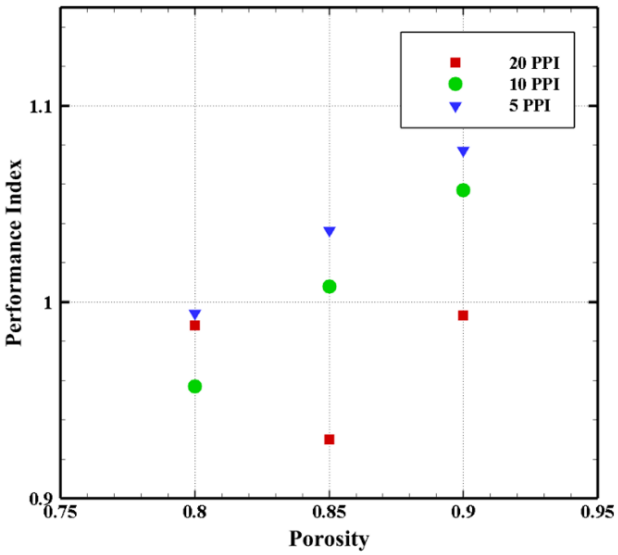


Fig. 7. Variation of performance index with respect to porosity as a result of using CuO/H_2O compared to Al_2O_3/H_2O

Nomenclature

Roman Symbols

g	Gravitational acceleration (m/s^2)
F	Interfacial force (N)
D	Diameter (m)
L	Length (m)
h	Coefficient of heat transfer (W/m^2K)
C	Inertial coefficient
k	Thermal conductivity (W/m K)

H	Enthalpy (J/kg)
T	Temperature (K)
u	Velocity (m/s)
P	Pressure (Pa)
q	Heat flux (kW/m^2)
Greek Symbols	
α	Viscous resistance
β	Accommodation coefficient
ε	Porosity
μ	Viscosity (kg/m s)
ρ	Density (kg/m^3)
σ	Surface tension (M/m)
ω	pore per inch (PPI)
τ	Shear stress (N/m^2)
∇	Vector gradient operator
Subscripts	
g	Vapor
l	Liquid
p	Pore
b	Bulk liquid
eff	Effective

6. References

[1] A. Kasaeian, R. Daneshazarian, O. Mahian, L. Kolsi and I. Pop, "Nanofluid flow and heat transfer in porous media: A review of the latest developments," *Heat and Mass Transfer*, vol. 107, pp. 778-791, 2017.

[2] J. Barber, D. Brutin, and L. Tadrist, "A review on boiling heat transfer enhancement with nanofluids," *Nanoscale Research Letters*, vol. 6, pp. 280, 2011.

[3] E. Abedini, A. Behzadmehr, H. Rajabnia, S. M. H. Sarvari, and S. H. Mansouri, "Experimental investigation and comparison of subcooled flow boiling of TiO2 nanofluid in a vertical and horizontal tube," *Proc. of the IMechE*, vol. 227, no. 8, pp. 1742–1753, Aug. 2013.

[4] Y. Wang and G. H. Su, "Experimental investigation on nanofluid flow boiling heat transfer in a vertical tube under different pressure conditions," *Experimental Thermal and Fluid Science*, vol. 77, pp. 116–123, Oct. 2016.

[5] S. Jaganathan, B. D. Naik, V. Ravikumar, R. Venkateshkumar, R. Dhairiyasamy, S. Rajendran and P. Alphonse, "Experimental investigation of the performance of silver nanofluid as a coolant in a helical shell and tube heat exchanger," *Journal of Thermal Analysis and Calorimetry*, vol. 149, no. 1, pp. 439–451, Jan. 2024.

[6] M. Hasheminia, M. H. Fard, S. Gholamreza Etemad, and S. H. Hashemabadi, "Forced Boiling of Nanofluids, Effects of Contact Angle and Surface Wettability," *Proc. of the 3rd Micro and Nano Flows Conference*, 2011.

[7] S. K. Das, N. Putra, and W. Roetzel, "Pool boiling of nano-fluids on horizontal narrow tubes," *International Journal of Multiphase Flow*, vol. 29, no. 8, pp. 1237–1247, 2003.

[8] M. Amani, M. Ameri, and A. Kasaeian, "The Experimental Study of Convection Heat Transfer Characteristics and Pressure Drop of Magnetite Nanofluid in a Porous Metal Foam Tube," *Transport in Porous Media*, vol. 116, no. 2, pp. 959–974, Jan. 2017.

[9] N. Dukhan, Ö. Baıci, and M. Özdemir, "Thermal development in open-cell metal foam: An experiment with constant wall heat flux," *International Journal of Heat and Mass Transfer*, vol. 85, pp. 852–859, 2015.

[10] M. Ghafarian, D. Mohebbi-Kalhori, and J. Sadeghi, "Analysis of heat transfer in oscillating flow through a channel filled with metal foam using computational fluid dynamics," *International Journal of Thermal Sciences*, vol.66, pp. 42–50, Apr. 2013.

[11] S. Azizifar, M. Ameri, and I. Behroyan, "Experimental investigation of the subcooled flow boiling heat transfer of water and nanofluids in a horizontal metal foam tube", *Heat and Mass Transfer*, vol. 57, pp. 1499-1511, 2021.

[12] S. Sivasankaran, M. A. Mansour, A. M. Rashad, and M. Bhuvaneswari, "MHD mixed convection of Cu–water nanofluid in a two-sided lid-driven porous cavity with a partial slip," *Numerical Heat Transfer*, vol. 70, no. 12, pp. 1356–1370, 2016.

[13] W. H. Lee, "A pressure iteration scheme for two-phase flow modeling", *Multiphase transport fundamentals, reactor safety, applications*, vol. 1, pp. 407-431, 1980.

[14] S. Sivasankaran and F. O. M. Mallawi, "Numerical study on convective flow boiling of nanoliquid inside a pipe filling with aluminum metal foam by two-phase model," *Case Studies in Thermal Engineering*, vol. 26, 101095, Aug. 2021.

[15] D. A. Nield, and A. Bejan, Convection in Porous Media, *Springer*, vol. 3, pp. 629-982, 2006.

[16] A. Rabiee and A. Atf, "A computational fluid dynamics investigation of various nanofluids in a boiling flow field," *Progress in Nuclear Energy*, vol. 95, pp. 61–69, Mar. 2017.